 MCB, vol.12, no.4, pp.249-263, 2015

Enhanced External Counterpulsation Treatment May Intervene The Advanced Atherosclerotic Plaque Progression by Inducing The Variations of Mechanical Factors: A 3D FSI Study Based on *in vivo* Animal Experiment

Jianhang Du[1,2,3], **Liang Wang**[4]

Abstract: Growing evidences suggest that long-term enhanced external counterpulsation (EECP) treatment can inhibit the initiation of atherosclerotic lesion by improving the hemodynamic environment in aortas. However, whether this kind procedure will intervene the progression of advanced atherosclerotic plaque remains elusive and causes great concern in its clinical application presently. In the current paper, a pilot study combining animal experiment and numerical simulation was conducted to investigate the acute mechanical stress variations during EECP intervention, and then to assess the possible chronic effects.

An experimentally induced hypercholesterolemic porcine model was developed and the basic hemodynamic measurement was performed *in vivo* before and during EECP treatment. Meanwhile, A 3D fluid-structure interaction (FSI) model of blood vessel with symmetric local stenosis was developed for the numerical calculation of some important mechanical factors. The results show that EECP augmented 12.21% of the plaque wall stress (PWS), 57.72% of the time average wall shear stress (AWSS) and 43.67% of the non-dimensional wall shear stress gradient ($WSSG_{nd}$) at throat site of the stenosis. We suggest that long-term EECP treatment may intervene the advanced plaque progression by inducing the significant variations of some important mechanical factors, but its proper effects will need a further research combined follow-up observation in clinic.

Keywords: Enhanced external couterpulsation, advanced plaque progression, fluid-

[1] School of Engineering, Guangdong Ocean University, Zhanjiang 524088, China
[2] Key laboratory on assisted circulation, Ministry of Health, Guangzhou 500089, China
[3] Corresponding Author: Jianhang Du, School of Engineering, Guangdong Ocean University, Zhanjiang 524088, China
[4] Mathematical Sciences Department, Worcester Polytechnics Institute, 100 Institute Road, Worcester, MA 01609, USA

structure interaction, plaque wall stress, flow shear stress.

1 Introduction

As a kind of non-invasive and atraumatic assisted circulation procedure, Enhanced external counterpulsation (EECP) has exhibited itself to be an effective, safe and economical therapy in clinic for the management of ischemic cardiovascular and cerebrovascular diseases in the recent decades [Manchanda and Soran (2007); Braith, Conti, Nichols, Choi, Khuddus, Beck and Casey (2010); Lin, Xiong, Han, Leung, Soo, Chen and Wong (2012); Liu, Xu, Wong, Wang and Wang (2014)], and has been introduced into the AHA/ACC Guideline of Coronary Artery Disease since 2002. The technique of EECP involves the use of the EECP device to inflate and deflate a seriesof compression cuffs wrapped around the patient's calves, lower thighs, and upper thighs, as showed as figure 1(a). As the result, the enhanced flow perfusion is derived from the device's propelling blood from veins of lower body to arteries of upper body and increases the blood supply for the important organs and brain.

Besides its advantage of improving the acute perfusion of vital organs through diastolic augmentation [Lin, Xiong, Han, Leung, Soo, Chen and Wong (2012)], EECP procedure has been demonstrated in former studies to be able to inhibit intimal hyperplasia and development of atherosclerosis by effectively improving the hemodynamic environment in aortas [Zhang, He, Chen, Ma, Liu, Luo, Du, Jin, Xiong, He et al. (2007); Yang and Wu (2013); Beck, Martin, Casey, Avery, Sardina and Braith (2014); DU, Wu, Zheng, Dai and feng (2014)]. However, considering that EECP treatment significantly induces elevated diastolic pressure in aortas, which will be even higher than systolic pressure, whether it will increase the potential risks of some acute and chronic hypertension-related events causes great concern in its clinical application [Lin, Xiong, Han, Leung, Soo, Chen and Wong (2012)]. But the relevant studies, especially the exact effects of long-term EECP treatment on the progression of advanced atherosclerotic plaque and its subsequent stability, are almost blank even to this day.

The instability and final rupture of atherosclerotic vulnerable plaque is responsible for most acute cardiac syndromes, including heart attack, myocardial infarction, and cerebral stroke. Although there is no general agreement has been found yet [Assemat, Armitage, Siu, Contreras, Dart, Chin-Dusting and Hourigan (2014)], the mechanical stresses in plaques are thought playing an important role in advanced plaque progression and the final rupture [Gijsen and Migliavacca (2014); Tang, Kamm, Yang, Zheng, Canton, Bach, Huang, Hatsukami, Zhu, Ma et al. (2014)], and can potentially be used for assessment of plaque vulnerability [Gijsen and Migliavacca (2014)]. Wall shear stress (WSS) exerted by blood flow and plaque

wall stress (PWS) induced by blood pressure are two mechanical factors that are thought correlating closely with plaque progression. The low and oscillatory WSS hypothesis for plaque formation and early progression has been proposed by numerous groups [Peiffer, Sherwin and Weinberg (2013); Chatzizisis, Baker, Sukhova, Koskinas, Papafaklis, Beigel, Jonas, Coskun, Stone, Maynard et al. (2011)]. Meanwhile, several studies suggested that the advanced plaque progression and final rupture might be associated with high WSS distribution [Groen, Gijsen, van der Lugt, Ferguson, Hatsukami, van der Steen, Yuan and Wentzel (2007); Yang, Canton, Yuan, Ferguson, Hatsukami and Tang (2010); Gijsen, van der Giessen, van der Steen and Wentzel (2013)]. However, considering the massive difference of the scale, structural stresses, such as PWS, are thought playing a more important role in advanced plaque process [Tang, Yang, Mondal, Liu, Canton, Hatsukami and Yuan (2008); Tang, Teng, Canton, Yang, Ferguson, Huang, Zheng, Woodard and Yuan (2009); Sadat, Teng and Gillard (2010)]. PWS shows a negative correlation with advanced plaque progression [Yang, Canton, Yuan, Ferguson, Hatsukami and Tang (2010); Gijsen, van der Giessen, van der Steen and Wentzel (2013); Tang, Yang, Mondal, Liu, Canton, Hatsukami and Yuan (2008)], and is suggested to be a better predictor of carotid plaque rupture sites than WSS [Tang, Teng, Canton, Yang, Ferguson, Huang, Zheng, Woodard and Yuan (2009); Sadat, Teng and Gillard (2010); Teng, Canton, Yuan, Ferguson, Yang, Huang, Zheng, Woodard and Tang (2010)]. A plaque is suggested to be unstable if its plaque cap stress (PCS) is in excess of a threshold value of 300 kPa, and cap thickness < 60 μm lead to PCS > 300 kPa [Williamson, Lam, Younis, Huang, Patel, Kaazempur-Mofrad and Kamm (2003)].

EECP treatment significantly induces the augmentation of aortic perfusion and blood pressure in cardiac cycles. We hypothesizes that it will affect the acute mechanical environment of advanced plaques, and in turn will chronically affect the subsequent progression. To understand the impact of biomechanical stimuli on advanced plaque during EECP intervention, a 3D fluid–structure interaction (FSI) model of blood vessel with symmetric stenosis was developed in the current paper, based on *in vivo* hemodynamic measurement performed in an experimentally induced hypercholesterolemic animal model.

2 Animal model and *in vivo* hemodynamic measurement

An experimentally induced hypercholesterolemic porcine model was developed in the current study. A male porket of 3-week-old, with the weight of 7.3kg, was fed with a high-cholesterol atherogenic diet containing 4% cholesterol, 10% yolk powder, 8% lard and 1.2% salts over a course of 15weeks, with the final weight of 45 kg, to initiate and accelerate the process of atherosclerotic lesion. At the end of the course, the *in vivo* hemodynamic measurement was performed before and

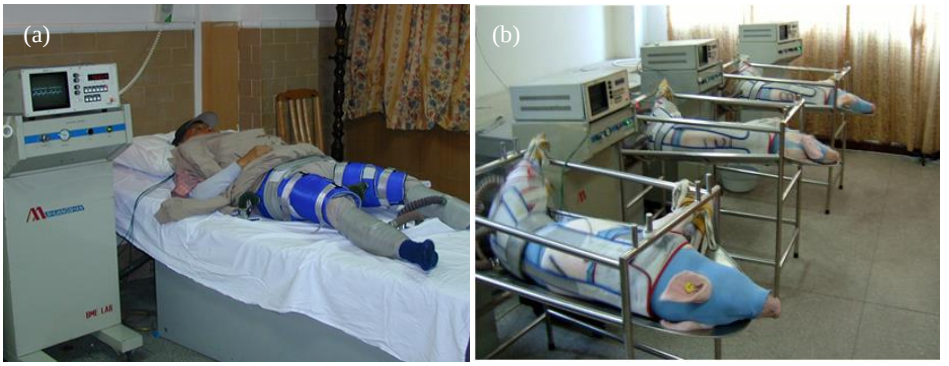

Figure 1: EECP treatment in clinic and animal experiment. (a) EECP in clinic. The technique involves the using of a set of cuffs that are wrapped around the lower parts of the body and connected to an air compressor with tubes. (b) Animal EECP experiment. The subjects were laid on their right sides and the cuffs were wrapped around their low extremities and hips.

during EECP treatment. The blood flow rate profiles were detected at left common artery using a Doppler ultrasound system (ATL-HDI-5000, Philip Com America) equipped with a 5–10 MHz multifrequency high-resolution linear probe. The blood pressure profiles were detected at left ventricular using the tip pressure transducer (TP-400T, NihonKohden, Japan). A clinical device system (Shuangshan EECP-MCI, Guangzhou, China) and specially designed experimental platform were used, as illustrated in Figure 1(b).

Figure 2 shows the measuring results of cardiogram and blood flow rate in three continuous cardiac cycles, before and during EECP treatment. The blood flow waveforms were used to solve the axial velocity distribution in the cardiac cycle based on the Womersley algorithm, which would serve as inflow boundary conditions in the following flow model.

3 The computational model

3.1 Geometrical model

A 3D idealized tube model with symmetric stenotic component was constructed, as illustrated as figure 3 (models were cut short for better viewing). Radius of the lumen of non-stenotic part was set to be 0.2cm, Length of the local stenosis was set to be 0.8cm, and lengths of proximal and distal sections were set to be 4cm (10 times of the lumen diameter of non-stenotic part).

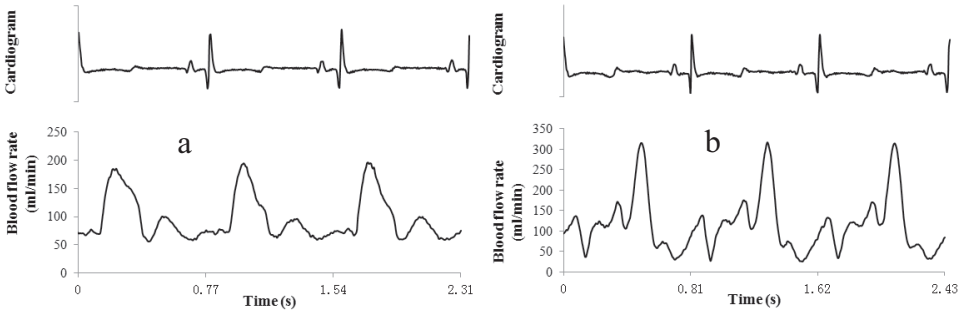

Figure 2: In vivo hemodynamic measurement. (a) Pre-EECP. (b) During EECP. Note that EECP intervention significantly changed the patterns of blood flow in cardiac cycles, and augmented the level of perfusion.

Define the stenosis severity normally as the following equation.

$$S_0 = \frac{R_0 - R_{\min}}{R_0} \times 100\%, \tag{1}$$

Then, the radius of the lumen at rest is specified as the following equation.

$$H_0(z) = R_0 - \begin{cases} \frac{1}{2} S_0 R_0 [1 - \cos(2\pi(z - z_1)/(z_2 - z_1))], & z_1 \le z \le z_2 \\ 0, & \text{otherwise} \end{cases} \tag{2}$$

Where R_0 is the radius of the lumen of non-steotic part; z_1 and z_2 are the beginning and ending positions of the stenotic part;

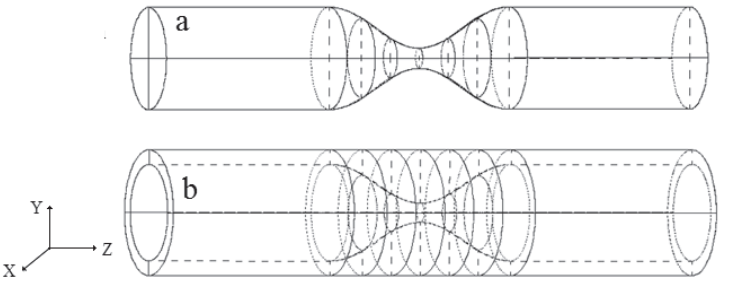

Figure 3: 3D Geometrical model of tube with local symmetric stenosis, S0 = 70%. (a) Flow lumen; (b) Wall structure.

3.2 Governing equations and boundary conditions

3.2.1 The flow model

Assuming that the blood flow was laminar, Newtonian, viscous, and incompressible. The incompressible Navier-Stokes equations with arbitrary Lagrangian-Eulerin (ALE) formulation were used as the governing equations, and are given as the following:

$$\rho(\partial \mathbf{u}/\partial t + ((\mathbf{u}-\mathbf{u}_g)\cdot\nabla)\mathbf{u}) = -\nabla p + \mu\nabla^2\mathbf{u}, \tag{3}$$

$$\nabla\cdot\mathbf{u} = 0, \tag{4}$$

$$\mathbf{u}|_\Gamma = (0,0,0), \tag{5}$$

Where $\mathbf{u}$ is flow velocity, $\mathbf{u}_g$ is mesh velocity, p is pressure, ρ is fluid density and μ isthe kinematical viscosity. Γ is the inner boundary of the lumen.

3.2.2 The wall model

Assuming that material for arterial wall is hyperelastic, isotropic, incompressible and homogeneous. The following equilibrium equations and boundary conditions were used for the wall model [Tang, Yang, Mondal, Liu, Canton, Hatsukami and Yuan (2008)].

$$\sigma^S_{ij,j} = 0, \tag{6}$$

$$\mathbf{d}^S\big|_{innerwall} = \mathbf{d}^f\big|_{innerwall}, \tag{7}$$

$$\sigma^S_{ij,j}\cdot n_j\big|_{innerwall} = \sigma^f_{ij,j}\cdot n_j\Big|_{innerwall}, \tag{8}$$

$$\sigma^S_{ij,j}\cdot n_j\big|_{outerwall} = 0, \tag{9}$$

Where $\mathbf{d}^S$, $\mathbf{d}^f$, $\sigma^S_{ij,j}$ and $\sigma^f_{ij,j}$ are displacement and stress tensors for solid and fluid respectively. Meanwhile, as the constraint conditions, the inlet and outlet face were fixed in axial (longitudinal) direction, but allowed to expand/contract with flow otherwise [Tang, Yang, Mondal, Liu, Canton, Hatsukami and Yuan (2008)].

3.2.3 Boundary conditions

The velocity and pressure boundary conditions were given to solve the FSI model. The Womersley method for pulsatile flow along a long and rigid circular vessel, as described as below, was introduced to solve the inlet axial velocity profiles in a cardiac cycle based on the *in vivo* measured blood flow rate waveform. The Womersley velocity profiles were used as the inlet boundary conditions for the solving of flow shear stress (FSS) and pressure drop of the model, before and during EECP treatment.

Performing a Fourier Transform to the blood flow rate waveform of a cardiac cycle:

$$Q(t) \approx \sum_{n=0}^{N} B_n e^{jn\omega t} \tag{10}$$

And then, the Womersley velocity for the axial component of velocity, $w(r,t)$ is given by

$$w(r,t) = \frac{2B_0}{\pi R_0^2}[1-(\frac{r}{R_0})^2] + \sum_{n=1}^{N} \frac{B_n}{\pi R_0^2}[(1-\frac{J_0(\alpha_n \frac{r}{R_0} j^{3/2})}{J_0(\alpha_n j^{3/2})})/(1-\frac{2J_1(\alpha_n j^{3/2})}{\alpha_n j^{3/2} J_0(\alpha_n j^{3/2})})]e^{jn\omega t} \tag{11}$$

Here, k is the number of the sequential flow rate discrete points in a cardiac cycle, $Q(t)$ is the flow rate, N is the order of the Fourier Transfer, $j=\sqrt{-1}$, $\omega = 2\pi/T$ is the angular frequency, T is the cardiac cycle, B_n is the Fourier coefficients, R_0 is the radius of the artery, α_n is known as the *Womersley number*, and $\alpha_n = R_0\sqrt{n\omega/\nu}$, ν is the kinematic viscosity of blood, $J_0\ldots$ and J_1 are Bessel function of the first kind of order 0 and 1.

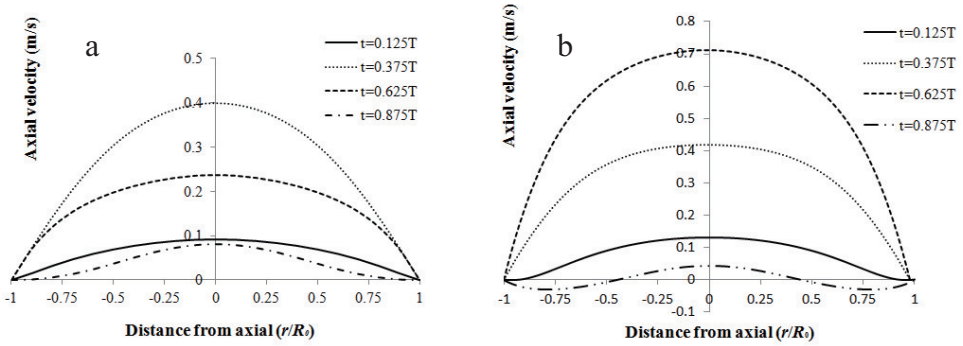

Figure 4: Womersley velocity profiles at different time points of a cardiac cycle. (a) Pre-EECP; (b) during EECP.

The pressure boundary conditions were given at inlet and outlet faces, as illustrated as figure 5, for the solving of structural stress and deformation of the wall. The inlet blood pressure profiles were measured *in vivo*. The outlet pressure profiles were calculated based on the inlet pressure and the pressure drops solved above.

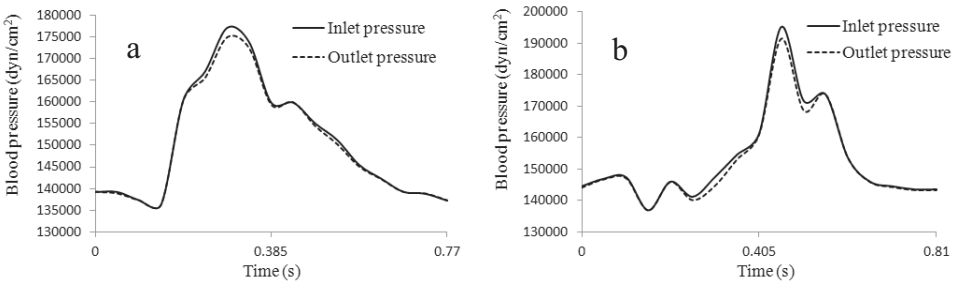

Figure 5: Pressure conditions specified at the inlet and outlet faces. (a) Pre-EECP; (b) During EECP.

3.3 Tissue properties

For the structural model, assuming that vessel wall is hyperelastic, isotropic, incompressible, and homogeneous. Then, the tissue propertie can be described by using the nonlinear modified Mooney-Rivlin model [Yang, Canton, Yuan, Ferguson, Hatsukami and Tang (2010); Tang, Yang, Mondal, Liu, Canton, Hatsukami and Yuan (2008)]. The strain energy function is given as following.

$$W = c_1(I_1 - 3) + c_2(I_2 - 3) + D_1[\exp(D_2(I_1 - 3)) - 1] \tag{12}$$

$$I_1 = \sum C_{ii}, \;\; I_2 = \frac{1}{2}[I_1^2 - C_{ij}C_{ij}] \tag{13}$$

Where I_1 and I_2 are the first and second strain invariants, $\mathbf{C} = [C_{ij}] = X^{\mathrm{T}}X$ is the right Cauchy-Green deformation tensor, $\mathbf{X} = [X_{ij}] = [\partial x_i/\partial a_j]$, (x_i) is current position, (a_i) is original position. c_i and D_i are material parameters. The stress-stretch curves derived from the modified Mooney-Rivlin model are illustrated as figure 6, where the material parameters are chosen based on Tang, Yang, Mondal, Liu, Canton, Hatsukami and Yuan (2008).

3.4 Computational solving strategy

The FSI models were solved by ADINA. ADINA uses unstructured finite element methods for both fluid and solid models. Nonlinear incremental iterative procedures are used to handle FSI. The governing finite element equations for both solid and fluid models were solved by Newton-Raphson iteration method [Tang, Yang, Mondal, Liu, Canton, Hatsukami and Yuan (2008); Tang, Teng, Canton, Yang, Ferguson, Huang, Zheng, Woodard and Yuan (2009)].

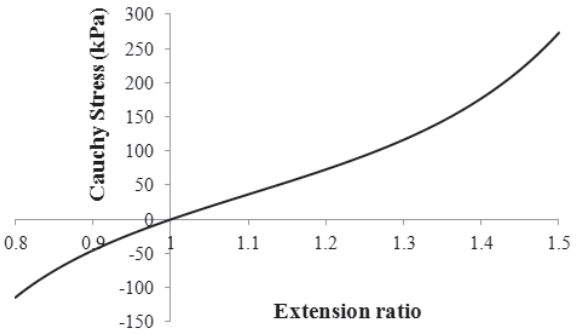

Figure 6: Material curve for the model. The parameters are: c1 = 368000, c2 = 0, D1 = 144000, D2 = 2.0.

4 Results

The distributions of both flow shear stress (FSS) and plaque wall stress (PWS) before and during EECP treatment were sold in a cardiac cycles, by using the FSI model developed above. FSS and PWS are two factors that are often used to represent the flow and structural stresses respectively.

The time average wall shear stress (AWSS) and the non-dimensional wall shear stress gradient ($\mathrm{WSSG_{nd}}$) are introduced as factors quantify the temporary average and special fluctuation of WSS over a cardiac cycle, which are given the as following equations [Murphy and Boyle (2010); Buchanan, Kleinstreuer, Truskey and Lei (1999)].

$$\mathrm{AWSS} = \frac{1}{T}\int_0^T |\vec{\tau}_w|\, dt; \tag{14}$$

$$\mathrm{WSSG} = \sqrt{(\left|\frac{\partial \vec{\tau}_w}{\partial x}\right|)^2 + (\left|\frac{\partial \vec{\tau}_w}{\partial y}\right|)^2 + (\left|\frac{\partial \vec{\tau}_w}{\partial z}\right|)^2} \tag{15}$$

$$\mathrm{WSSG_{nd}} = \frac{1}{T}\frac{d_0}{\tau_0}\int_0^T |\mathrm{WSSG}|dt; \tag{16}$$

The following figures show the simulation results of the mechanical factors in symmetric profile of longitudinal direction (X-cut). The distributions of flow shear stress (FSS) and structural stress before and during EECP treatment are involved. In the current paper, the maximum principal stress was used to characterise the stress condition of the structure.

The following figure (figure 9) show the distributions of AWSS and $\mathrm{WSSG_{nd}}$ along the longitudinally symmetric line on the inner wall of the structural model.

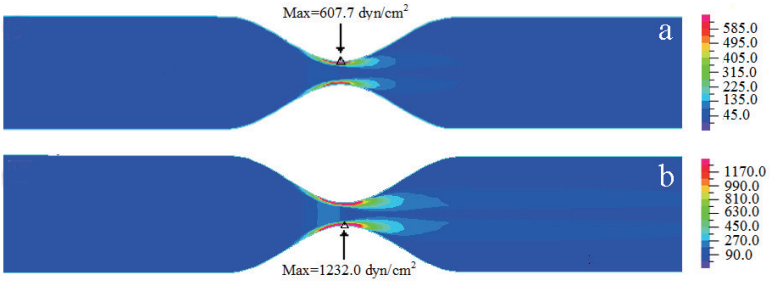

Figure 7: Flow shear stress (FSS) distributions, x-cut profile. (a) Pre-EECP, t = 35T/130; (b) During EECP, t = 80T/132.

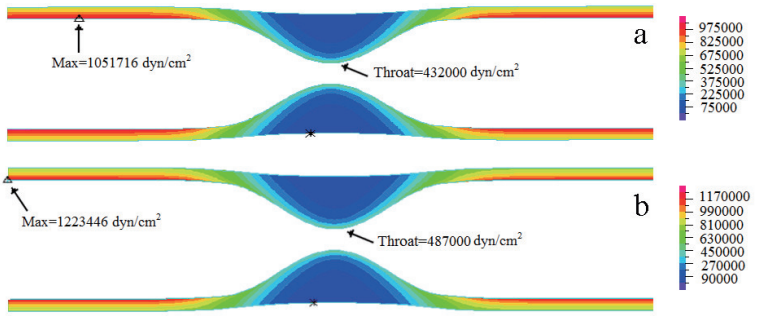

Figure 8: Structural stress distributions, x-cut profile. (a) Pre-EECP, t = 35T/130; (b) During EECP, t = 80T/132.

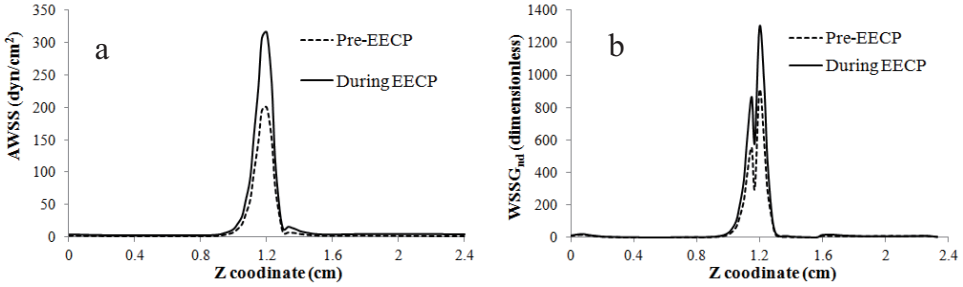

Figure 9: Wall shear stress and its spacial oscillation over a cardiac cycle. (a) AWSS before and during EECP; (b) $WSSG_{nd}$ before and during EECP.

According to the simulation results, the peak structural stresses appeared at upstream site of the local stenosis in both cases of before and during EECP, and the local stenotic site showed lower level of structural stress distribution. EECP inter-

vention significantly changed the distribution characteristics of the structural stress in cardiac cycle and augmented its level. During EECP treatment, the peak value of the structural stress (1223446 dyn/cm^2) happened in diastole ($t = 80T/132$). Correspondingly, the structural stress at the middle of the stenosis (throat site) was 487000 dyn/cm^2 at that time point during EECP. Whereas, the peak value of the structural stress before EECP treatment (1051716 dyn/cm^2) happened in systole ($t = 35T/130$). And at that time point, the structural stress at the middle of the stenosis (throat site) was 432000 dyn/cm^2. EECP treatment increased 12.21% of the structural stress at the middle of the stenosis, compared with the normal physiological status (before EECP).

Meanwhile, the peak FSS values appeared at the throat of the stenotic site in both cases of before and during EECP, and the non-stenotic sites were where lower FSS level distributed. During EECP treatment, the peak FSS value (1232.0 dyn/cm^2) happened in diastole ($t = 80T/132$), compared with that of 607.7 dyn/cm^2 before EECP which happened in systole ($t = 35T/130$). The peak FSS value during EECP augmented 102.73% compared to that of before EECP.

Finally, both AWSS and WSSG_{nd} showed higher-level distributions in local stenotic site. The peak values of AWSS over a cardiac cycle, which appeared at the throat site of the steosis, were 315.74 dyn/cm^2 (during EECP) and 200.19 dyn/cm^2 (before EECP) respectively. The peak values of WSSG_{nd} over a cardiac cycle, which appeared at the throat site of the steosis, were 1298.05 (during EECP) and 903.47(before EECP) respectively. EECP intervention induced an augmentation of 57.72% of AWSS level and an augmentation of 43.67% of WSSG_{nd} level compared to that of before EECP.

5 Conclusions

The pilot study of the present paper aimed to explore the influence of EECP treatment, which has been introduced into the AHA/ACC Guideline of Coronary Artery Disease for over ten years, on flow and structural stress conditions of blood vessel with advanced plaque. The study was conducted based on a combination of *in vivo* animal experiment and 3D numerical simulation.

The stress conditions are thought playing important roles in the progression of the plaque and its final rupture. Many studies suggested that PWS showed a negative correlation with plaque progression [Yang, Canton, Yuan, Ferguson, Hatsukami and Tang (2010); Tang, Yang, Mondal, Liu, Canton, Hatsukami and Yuan (2008); Tang, Teng, Canton, Yang, Ferguson, Huang, Zheng, Woodard and Yuan (2009); Sadat, Teng and Gillard (2010)]. Meanwhile, some studies suggested that FSS/WSS might play a positive correlation with advanced plaque progression [Yang,

Canton, Yuan, Ferguson, Hatsukami and Tang (2010); Gijsen, van der Giessen, van der Steen and Wentzel (2013)], yet in others, lower FSS/WSS was thought contributing to continued plaque progression [Tang, Yang, Mondal, Liu, Canton, Hatsukami and Yuan (2008)]. Considering the massive difference of the scale, structural stress was thought to be a more critical stress factor that affected advanced plaque progression than FSS/WSS [Sadat, Teng and Gillard (2010)]. The results obtained in the present paper show that EECP treatment induces significant augmentations of the instant level of both FSS/WSS and structural stress (PWS) at the local stenotic site, as well as their characteristics of distributions in cardiac cycles. We thus suggest that long-term EECP treatment may intervene the advanced atherosclerotic plaque progression by inducing the variations of mechanical factors. However, either EECP treatment may play a positive effect on inhibiting the continued plaque progression by increasing the PWS level to some extent, or a negative effect by increasing the WSS level and its spatial oscillation, which will need further studies combined with clinical observations.

6 Limitations

In the present pilot study, the conclusions were obtained based on idealized blood vessel model with symmetric stenosis of plaque, and the components of the plaque were not taken into account. The geometries and the plaque components, especially the lipid pool and fibrous cap, are thought having influences on the critical FSS and structural stress [Tang, Yang, Mondal, Liu, Canton, Hatsukami and Yuan (2008); Tang, Teng, Canton, Yang, Ferguson, Huang, Zheng, Woodard and Yuan (2009); Teng, Canton, Yuan, Ferguson, Yang, Huang, Zheng, Woodard and Tang (2010); Yuan, Teng, Feng, Zhang, Brown, Gillard, Jing and Lu (2015)]. Attempt will be made in our future work to improve the model.

Acknowledgement: The present research is supported by the Key Clinical Project from the Ministry of Health (25400) and the National Natural Science Foundation of China (81170272).

References

Assemat, P.; Armitage, J. A.; Siu, K. K.; Contreras, K. G.; Dart, A. M.; Chin-Dusting, J. P.; Hourigan, K. (2014): Three-dimensional numerical simulation of blood flow in mouse aortic arch around atherosclerotic plaques. *Applied Mathematical Modelling*, vol. 38, no. 17, pp. 4175–4185.

Beck, D. T.; Martin, J. S.; Casey, D. P.; Avery, J. C.; Sardina, P. D.; Braith, R. W. (2014): Enhanced external counterpulsation improves endothelial function

and exercise capacity in patients with ischaemic left ventricular dysfunction. *Clinical and Experimental Pharmacology and Physiology*, vol. 41, no. 9, pp. 628–636.

Braith, R. W.; Conti, C. R.; Nichols, W. W.; Choi, C. Y.; Khuddus, M. A.; Beck, D. T.; Casey, D. P. (2010): Enhanced external counterpulsation improves peripheral artery flow-mediated dilation in patients with chronic angina a randomized sham-controlled study. *Circulation*, vol. 122, no. 16, pp. 1612–1620.

Buchanan, J. R.; Kleinstreuer, C.; Truskey, G. A.; Lei, M. (1999): Relation between non-uniform hemodynamics and sites of altered permeability and lesion growth at the rabbit aorto-celiac junction. *Atherosclerosis*, vol. 143, no. 1, pp. 27–40.

Chatzizisis, Y. S.; Baker, A. B.; Sukhova, G. K.; Koskinas, K. C.; Papafaklis, M. I.; Beigel, R.; Jonas, M.; Coskun, A. U.; Stone, B. V.; Maynard, C. et al. (2011): Augmented expression and activity of extracellular matrix-degrading enzymes in regions of low endothelial shear stress colocalize with coronary atheromata with thin fibrous caps in pigs. *Circulation*, vol. 123, no. 6, pp. 621–630.

DU, J.-h.; Wu, G.-f.; Zheng, Z.-s.; Dai, G.; feng, M.-z. (2014): Enhanced external counterpulsation inducing arterial hemodynamic variations and its chronic effect on endothelial function. *Chinese Journal of Biomedical Engineering*, vol. 3, pp. 006.

Gijsen, F.; Migliavacca, F. (2014): Plaque mechanics. *Journal of biomechanics*, vol. 47, no. 4, pp. 763.

Gijsen, F.; van der Giessen, A.; van der Steen, A.; Wentzel, J. (2013): Shear stress and advanced atherosclerosis in human coronary arteries. *Journal of biomechanics*, vol. 46, no. 2, pp. 240–247.

Groen, H. C.; Gijsen, F. J.; van der Lugt, A.; Ferguson, M. S.; Hatsukami, T. S.; van der Steen, A. F.; Yuan, C.; Wentzel, J. J. (2007): Plaque rupture in the carotid artery is localized at the high shear stress region a case report. *Stroke*, vol. 38, no. 8, pp. 2379–2381.

Lin, W.; Xiong, L.; Han, J.; Leung, T. W. H.; Soo, Y. O. Y.; Chen, X.; Wong, K. S. L. (2012): External counterpulsation augments blood pressure and cerebral flow velocities in ischemic stroke patients with cerebral intracranial large artery occlusive disease. *Stroke*, vol. 43, no. 11, pp. 3007–3011.

Liu, L.-P.; Xu, A.-D.; Wong, L. K.; Wang, D. Z.; Wang, Y.-J. (2014): Chinese consensus statement on the evaluation and intervention of collateral circulation for ischemic stroke. *CNS neuroscience & therapeutics*, vol. 20, no. 3, pp. 202–208.

Manchanda, A.; Soran, O. (2007): Enhanced external counterpulsation and future directions: step beyond medical management for patients with angina and

heart failure. *Journal of the American College of Cardiology*, vol. 50, no. 16, pp. 1523–1531.

Murphy, J.; Boyle, F. (2010): Predicting neointimal hyperplasia in stented arteries using time-dependant computational fluid dynamics: a review. *Computers in biology and medicine*, vol. 40, no. 4, pp. 408–418.

Peiffer, V.; Sherwin, S. J.; Weinberg, P. D. (2013): Does low and oscillatory wall shear stress correlate spatially with early atherosclerosis? a systematic review. *Cardiovascular research*, vol. 99, pp. 242–250.

Sadat, U.; Teng, Z.; Gillard, J. H. (2010): Biomechanical structural stresses of atherosclerotic plaques. *Expert review of cardiovascular therapy*, vol. 8, no. 10, pp. 1469–1481.

Tang, D.; Kamm, R. D.; Yang, C.; Zheng, J.; Canton, G.; Bach, R.; Huang, X.; Hatsukami, T. S.; Zhu, J.; Ma, G. et al. (2014): Image-based modeling for better understanding and assessment of atherosclerotic plaque progression and vulnerability: Data, modeling, validation, uncertainty and predictions. *Journal of biomechanics*, vol. 47, no. 4, pp. 834–846.

Tang, D.; Teng, Z.; Canton, G.; Yang, C.; Ferguson, M.; Huang, X.; Zheng, J.; Woodard, P. K.; Yuan, C. (2009): Sites of rupture in human atherosclerotic carotid plaques are associated with high structural stresses an in vivo mri-based 3d fluid-structure interaction study. *Stroke*, vol. 40, no. 10, pp. 3258–3263.

Tang, D.; Yang, C.; Mondal, S.; Liu, F.; Canton, G.; Hatsukami, T. S.; Yuan, C. (2008): A negative correlation between human carotid atherosclerotic plaque progression and plaque wall stress: in vivo mri-based 2d/3d fsi models. *Journal of biomechanics*, vol. 41, no. 4, pp. 727–736.

Teng, Z.; Canton, G.; Yuan, C.; Ferguson, M.; Yang, C.; Huang, X.; Zheng, J.; Woodard, P. K.; Tang, D. (2010): 3d critical plaque wall stress is a better predictor of carotid plaque rupture sites than flow shear stress: an in vivo mri-based 3d fsi study. *Journal of biomechanical engineering*, vol. 132, no. 3, pp. 031007.

Williamson, S.; Lam, Y.; Younis, H.; Huang, H.; Patel, S.; Kaazempur-Mofrad, M.; Kamm, R. (2003): On the sensitivity of wall stresses in diseased arteries to variable material properties. *Journal of biomechanical engineering*, vol. 125, no. 1, pp. 147–155.

Yang, C.; Canton, G.; Yuan, C.; Ferguson, M.; Hatsukami, T. S.; Tang, D. (2010): Advanced human carotid plaque progression correlates positively with flow shear stress using follow-up scan data: an in vivo mri multi-patient 3d fsi study. *Journal of biomechanics*, vol. 43, no. 13, pp. 2530–2538.

Yang, D.-y.; Wu, G.-f. (2013): Vasculoprotective properties of enhanced external counterpulsation for coronary artery disease: beyond the hemodynamics. *International journal of cardiology*, vol. 166, no. 1, pp. 38–43.

Yuan, J.; Teng, Z.; Feng, J.; Zhang, Y.; Brown, A. J.; Gillard, J. H.; Jing, Z.; Lu, Q. (2015): Influence of material property variability on the mechanical behaviour of carotid atherosclerotic plaques: A 3d fluid-structure interaction analysis. *International journal for numerical methods in biomedical engineering*, vol. 31, no. 8.

Zhang, Y.; He, X.; Chen, X.; Ma, H.; Liu, D.; Luo, J.; Du, Z.; Jin, Y.; Xiong, Y.; He, J. et al. (2007): Enhanced external counterpulsation inhibits intimal hyperplasia by modifying shear stress–responsive gene expression in hypercholesterolemic pigs. *Circulation*, vol. 116, no. 5, pp. 526–534.